Check for updates

Formulation and evaluation of PVA-sucrose dissolving microneedles loaded with glimepiride nanocrystals as a potential transdermal delivery system

Walhan Alshaer, [ID] [a] Ayman Alhaj Abbas, [ID] [b] Yazan Al Thaher, [ID] [c] Hatim Alkhatib,[b] Samir Jabaiti,[d] Ola Tarawneh,[e] Rula Al-Buqain[a] and Sharif Abdelghany [ID] *[b]

Considering the limited research on microneedles for potent transdermal oral hypoglycemic drugs, in this study, we formulated, glimepiride nanocrystals and incorporated them into PVA-based, sucrose-dissolving microneedles. Nanocrystals were formulated using two different aqueous surfactant solutions as antisolvents, PVP (at concentrations of 0.2% w/v or 2.5% w/v) and SLS (0.2% w/v), with or without a post-drying grinding step. Glimepiride nanocrystals using 0.2% w/v SLS with grinding showed the smallest particle size of 348 ± 27 nm with a PI of 0.29 ± 0.05, which was confirmed by SEM imaging. Therefore, the SLS-with-grinding formula was used for incorporation into a polymeric microneedle formulation composed of 23% w/w PVA and 15% w/w sucrose (GLIM_MN). GLIM_MN showed a microneedle height of 500 ± 14 μm and a sharp tip, as shown under SEM imaging. Furthermore, GLIM_MN could withstand a force of 32 N for 30 seconds at a rate of 0.5 mm per second. Moreover, GLIM_MN successfully penetrated three layers of Parafilm, which is analogous to the mechanical properties of the skin, and successfully penetrated excised BALB/c mice skin to a depth of 480 ± 15 μm, as shown by bright-field image microscopy. Moreover, GLIM_MN showed full penetration of the array into excised human skin to a depth of 276 ± 65 μm. Subsequently, we monitored the glucose level in healthy BALB/c mice for over 24 hours. The GLIM_MN treated group showed a rapid decline in the blood glucose level, reaching a minimum level at 5 hours. This was also corroborated with an increase in the level of serum insulin in the GLIM_MN treated group compared with that in the untreated group 5 hours after administration. Moreover, GLIM_MN-treated mice showed no significant change in the serum C-reactive protein level compared with that in the untreated group, indicating no inflammation upon microneedle administration. These results collectively indicate that our glimepiride dissolving microneedle formulation can enhance the delivery of glimepiride with minimal invasiveness, causing no inflammation. Therefore, it can be considered a potential treatment in the management of type 2 diabetes mellitus, avoiding the drawbacks associated with conventional oral administration.

1. Introduction

Over the past few decades, the number of adults living with diabetes mellitus worldwide has increased fivefold from 108 million in 1980 to 537 million and caused 6.7 million deaths in 2021.[1] An estimated 90% of diabetic adults have type 2 diabetes.[2] The management of type 2 diabetes mellitus includes lifestyle improvement, oral medications, and insulin therapy.[3]

[a]*Cell Therapy Center, University of Jordan, Amman, 11942, Jordan*

[b]*Department of Pharmaceutics and Pharmaceutical Technology, School of Pharmacy, University of Jordan, Amman, 11942, Jordan. E-mail: s.abdelghany@ju.edu.jo*

[c]*Faculty of Pharmacy, Philadelphia University, Amman, 19392, Jordan*

[d]*Department of Plastic Surgery, School of Medicine, University of Jordan, Amman, 11942, Jordan*

[e]*Faculty of Pharmacy, Al-Zaytoonah University of Jordan, Amman, Jordan*

Glimepiride is an oral medication used to manage and treat type 2 diabetes mellitus. This drug is a second-generation sulfonylurea insulin secretagogue class of drugs. It works by blocking ATP-sensitive potassium channels (KATP channels), causing depolarization of the pancreas's beta cells, resulting in insulin secretion.[4,5] Besides its pancreatic effect, glimepiride has been shown to reduce insulin resistance and increase hepatic glucose disposal in animal models.[6] It is administered as monotherapy in type 2 diabetic patients with no glycemic control by dietary and lifestyle modifications.[7] Compared with other sulfonylureas, glimepiride has been shown to be associated with a lower incidence of hypoglycemia.[8]

Previously, transdermal delivery of oral antidiabetic drugs was studied since it bypasses the first pass effect and provides less potential for hypoglycemia.[9,10] Moreover, many advantages

Paper

have been found for transdermal drug delivery systems, including minimal peak concentration and reduced dosing frequencies, which leads to improved patient compliance.[11] Compared to oral drug delivery and injectable drugs, transdermal drug delivery has significantly contributed to reaching the target through permeation and/or penetration of the stratum corneum *via* microneedles and other electroporation techniques.[12] Microneedle-based drug delivery systems have previously shown great promise for managing diabetes mellitus.[13] Many previous studies have focused on the delivery of smart glucose sensing and insulin through microneedles as a painless and noninvasive drug delivery system.[11,14] Moreover, for type 2 diabetes mellitus, oral antidiabetic drugs can be loaded into dissolvable microneedles to provide a longer hypoglycemic effect compared to subcutaneous application.[15] This is due to the ability of dissolving microneedles to penetrate the stratum corneum, the uppermost layer of the skin, and dissolve within deeper layers, releasing the incorporated drug over a prolonged period.[16] The stratum corneum is composed of dead keratinized cells that result from the final differentiation of deeper viable epidermal keratinocytes, providing a hydrophobic shield for deeper layers from the external environment.[17] Dissolving microneedles are arrays of ultra-small needles made from water-soluble polymers of less than 1000 μm intended to dissolve after application and penetrate the stratum corneum with minimal invasiveness.[18] Dissolving polymeric microneedles have several advantages that include the ease of preparation and disposal, and have relatively high drug loading capability compared to other types of microneedles.[19]

Glimepiride is a second-generation sulfonylurea widely used for the management of type 2 diabetes mellitus. Although it is conventionally administered orally, this route presents several pharmacokinetic and safety-related limitations. One major concern is extensive first-pass hepatic metabolism, which not only reduces the bioavailability of the drug, but also contributes to interindividual variability in therapeutic response.[20] Additionally, oral glimepiride has been associated with gastrointestinal side effects and a risk of dose-dependent hypoglycemia, particularly when plasma concentrations peak rapidly following absorption.[21] These issues underscore the need for alternative delivery strategies that can bypass the gastrointestinal tract, while maintaining controlled and sustained drug release. Transdermal delivery *via* dissolving microneedles offers a promising solution by enabling direct transport of the drug into systemic circulation, thus avoiding first-pass metabolism and improving pharmacokinetic control.[22] Moreover, dissolving microneedles are minimally invasive, pain-free, and can be self-administered, which may improve patient compliance and adherence for elderly patients, dysphagia populations, or needle-averse populations.[23,24]

This study describes the development and evaluation of a dissolving microneedle (MN) system based on a PVA/sucrose matrix incorporating glimepiride nanocrystals to improve transdermal delivery for diabetes treatment. We thoroughly evaluated the microneedles' mechanical properties with Parafilm®, excised murine skin, and excised human skin samples as penetrative models. In addition, we studied the *in vivo* antidiabetic efficacy of glimepiride-loaded microneedles in BALB/c mice by evaluating the changes in blood glucose and serum insulin levels over time. To evaluate the possible advantages of transdermal delivery, the therapeutic performance of the MN formulation was compared to that of glimepiride administered orally and at an equivalent dose.

2. Materials and methods

2.1. Materials

Glimepiride, fully hydrolyzed poly(vinyl alcohol) (PVA), and sucrose were purchased from Merck, Germany. Dimethyl formamide (DMF) was purchased from Labkem, Spain. Methylene blue hydrate, phosphate buffer 1× tablets, acetonitrile, hematoxylin and eosin, polyvinyl pyrrolidone (average molecular weight 10 000 (PVP)), and carrageenan sodium salt were purchased from Sigma Aldrich-Germany. Sodium lauryl sulfate (SLS) was purchased from Biochem Chemopharma, France. Double-distilled HPLC-grade water was used for this study.

2.2. Analysis of glimepiride content

The analysis of glimepiride was adopted from Mohd *et al.*, 2014,[25] with modifications and performed using HPLC (Shimadzu HPLC, model LC-2030C PLUS 3D). The system included an integrated solvent and degasser, an analytical pump, a thermostat autosampler, a thermostatic column compartment, and a UV detector. Data acquisition was conducted using the LabSolutions LCGC program. The eluent was monitored at 228 nm. Chromatographic separation was carried out at 25 °C using a reversed-phase Interclone® C18 column (250 mm × 4.6 mm, 5 μm particle ODS 100 Å size) (Phenomenex®, California, USA). The mobile phase had an isocratic composition of acetonitrile: 0.2 M phosphate buffer (pH = 7.4), 40 : 60 v/v, eluted at a 1 mL min⁻¹ flow rate. The injection volume was set at 20 μL. The drug concentration in each sample was then determined according to a calibration curve. This calibration curve was constructed by correlating peak areas measured with the known concentrations of glimepiride solutions. All measurements were conducted in triplicate to calculate the mean values and standard deviations.

2.3. Preparation of the glimepiride nanosuspension

The glimepiride nanosuspension was prepared using a direct nanoprecipitation method employing probe sonication. Dimethylformamide (DMF) was used as a solvent and distilled water containing a stabilizer was used as the antisolvent. A 400 μL volume of 12.5 mg mL⁻¹ glimepiride, dissolved in DMF, was added to an aqueous solution composed of 5 mL of 0.2% w/v PVP (F1), 5 mL of 2.5% w/v PVP (F2), or 5 mL of 0.2% w/v SLS under stirring (MS-H-S10, Dragonlab, China). The sonication was performed for 5 min at an amplitude of 90% (90 W) on pulse mode using a probe sonicator (UP200Ht, Hielscher, Germany). Finally, the suspension was centrifuged at 9000 rpm for 10 min using a small benchtop centrifuge (Heraeus Megafuge, Thermofisher, Germany). The supernatant was discarded, and the nanocrystals were resuspended in HPLC-grade distilled

water. The formed nanocrystals were then dried at room temperature under vacuum. For the 0.2% SLS formula, two formulations were prepared; one without a mortar and pestle size reduction step, and the other with a mortar and pestle size reduction step, where the dry powder was ground using a mortar and pestle for 5 minutes.

2.4. Nanocrystal characterization

The particle size and polydispersity index (PI) were measured using dynamic light scattering (3000 HS; Malvern Instruments, Malvern, UK). Measurements were performed using a monochromatic coherent He–Ne laser light of a fixed wavelength (633 nm) at 90° and room temperature. Each particle size measurement was done in triplicate. Formulations were suspended in 5 mL of distilled water by sonication on pulse mode for 2 minutes at 90% (90 W) using a probe sonicator (UP200Ht, Hielscher, Germany) to measure the particle size.

The SLS nanocrystal formulations were imaged using scanning electron microscopy (SEM). First, nanocrystal samples were spread on aluminum foil and dried for one day at room temperature under vacuum. Subsequently, nanocrystal samples were mounted on carbon adhesive-coated stubs and imaged under a scanning electron microscope (HiVac, 3 kV using Versa 3D, FEI, Netherlands).

Differential scanning calorimetric analysis (DSC) for glimepiride, ground glimepiride nanocrystals and SLS was performed utilizing a Mettler Toledo DSC823e (Mettler, Switzerland) by heating 2 to 3 mg of each compound in an aluminum crucible from 25 °C to 350 °C, at a heating rate of 10 °C min^{-1} and nitrogen flow of 80 mL min^{-1} with an empty aluminum crucible as a reference.

Furthermore, thermogravimetric analysis (TGA) was conducted using a Mettler Toledo TGA/DSC instrument (Mettler Toledo, Zurich, Switzerland) for the same compounds. Each sample was placed inside an alumina crucible heated at a heating rate of 10 °C min^{-1} in the temperature range from 30 to 800 °C under a nitrogen flow (60 mL min^{-1}).

2.5. Preparation of microneedles loaded with ground glimepiride nanocrystals

Microneedles loaded with the 0.2% SLS ground formula of glimepiride nanocrystals (GLIM_MN) were prepared using two-layer centrifugation. Briefly, 8 mg of ground glimepiride nanocrystals and 4 g of 23% w/w PVA/15% w/w sucrose aqueous solution were stirred using a magnetic stirrer at 75 °C (MS-H-S10, Dragonlab, China). The prepared polymeric mixture was then poured into 15 × 15, poly(dimethylsiloxane) (PDMS) microneedle molds, measuring 600 μm in depth and 200 μm in base length. Then, the molds were centrifuged at 2500 rpm for 20 min to fill the holes of the molds using a benchtop centrifuge (Heraeus Megafuge, Thermofisher, Germany). The excess mixture was removed using a spatula, and the molds were left for 24 hours at room temperature to dry the needles. The aqueous-based polymeric solution of 23% w/w PVA was added to the molds and centrifuged at 2500 rpm for 20 min. The microneedles were left for 24 hours to dry and then gently

removed from the molds. Methylene blue-loaded microneedles were prepared in a similar manner; however, with the addition and stirring of 2 mg of methylene blue dye to the PVA/sucrose blend prior to pouring onto the PDMS molds in the initial step. Blank microneedles (Blank_MN) were prepared in a similar way to GLIM_MN, omitting the addition of glimepiride.

2.6. Characterization of microneedles

The length of the microneedles was initially measured using a bright-field microscope (Carl Zeiss Microscopy, Germany). Subsequently, the mechanical strength of the microneedles loaded with ground glimepiride nanocrystals was investigated. Briefly, the tips of the microneedle array loaded with ground nanocrystals (0.2% SLS formula) were directed upward on the base surface of the texture analyser (EZ-LX, Shimadzu, Japan), and pressed with the shaft at a rate of 0.5 mm s^{-1} for 30 s and a force of 32 N (0.142 N/needle). Then, the morphological changes were observed using a bright-field microscope. The penetration of the microneedles into the Parafilm® was examined by tightly stacking 8 layers of Parafilm and placing the layers over dental wax. Subsequently, the GLIM_MN formula was applied using a thumb press. The created pores were visualized under a digital light microscope (DM4 Digital Microscope, China). SEM was also used to image GLIM_MN by mounting the microneedle sample on carbon adhesive-coated stubs and imaging was performed under HiVac, 3 kV using Versa 3D, FEI, Netherlands. The glimepiride content in the microneedles was determined by cutting the microneedles and dissolving them using the mobile phase, and the obtained solution was subjected to HPLC analysis after filtration.

2.7. Histological study

Excised murine skin and excised human skin were used to study the insertion capability of the prepared microneedles. The excised human skin specimen was obtained from a 38-year-old female undergoing abdominal plastic surgery at the Jordan University Hospital. Informed consent was obtained from the participant, and all procedures were performed in accordance with the Declaration of Helsinki and approved by the ethics committee at the Jordan University Hospital (Ethical approval No. 406/2021). The obtained skin was treated as previously described for earlier obtained specimens.[26] Specimens were defatted using a scalpel, cleaned by tapping with dry wipes, and placed onto a paperboard wrapped with aluminum foil, and the skin surface was oriented upward. The skin was then kept in zipper plastic bags and stored at −80 °C with an expiry date of 6 months from the date of obtaining the skin. In parallel, murine skin was excised from 4–6-week-old female mice (BALB/c). All procedures and experiments conducted on the BALB/c mice in this study were performed in accordance with the Guidelines for the Care and Use of Laboratory Animals of the University of Jordan, and the experiments were approved by the Animal Ethics Committee at the Deanship of Scientific Research, University of Jordan (Ethical Approval No. 82-2022). Shaved

mice skin samples were stored in a sealed weighing boat at −20 °C until use.

After the insertion of the microneedle array inside the human or murine skin, skin samples were stored at −20 °C for histological examination. Then, they were sectioned into slices of 5 μm thickness using a paraffin embedding procedure, in which tissues were fixed by immersion in 10% buffered formalin. Subsequently, they were processed using a tissue processer (Thermo Electron Shandon Citadel 2000 Tissue Processor, UK) with increasing concentrations of ethanol as a dehydration step and to remove any formalin remnant, followed by immersion in xylene to remove ethanol from the tissues and to prepare them for the paraffin infiltration step. Finally, they were embedded in paraffin wax for solidification into paraffin blocks. The paraffin blocks were cooled with ice for 15 min to be sectioned using an automatic rotary microtome (Thermo Scientific HM 355 S automatic rotary microtome, Germany), and the sliced samples containing tissues were stained using hematoxylin and eosin. Bright field images were taken for the stained sectioned samples to detect the depths at which the needles pierced both excised murine skin and excised human skin.

2.8. Microneedle dissolution in the murine skin

Shaved mice skin samples were stored in a sealed weighing boat at −20 °C until use. One section of full-thickness mice skin was placed onto a piece of tissue paper in a weighing boat, and wetted with PBS to prevent drying out. GLIM_MN was applied to the skin and manually applied to the skin, with 10 g weight applied on the top of the array to avoid microneedle expulsion. GLIM-MN were withdrawn from the skin at predefined time points, and their heights were measured using a bright-field microscope.

2.9. Microneedles release study

A Franz diffusion cell setup was used to evaluate glimepiride's *in vitro* drug release profile from dissolving microneedles. The receptor chamber was filled with phosphate-buffered saline (PBS, pH 7.4) containing 10% w/v Tween 80 and maintained at 37 °C using a water jacket system. Excised mice skin was secured over the receptor compartment, ensuring proper alignment and the absence of air bubbles. The microneedle patch was applied onto the mice skin in the donor compartment, and a cylindrical 10 g metal weight was placed on the top of the applied microneedles to avoid expulsion. The donor compartment was then sealed with Parafilm to prevent evaporation. Samples of 0.2 mL were withdrawn from the receptor chamber at predetermined time points, and replaced with fresh release media to maintain sink conditions. The collected samples were analyzed for glimepiride content using the above HPLC method, and the cumulative amount of permeated drug was plotted against time.

2.10. *In vivo* study on mice

In vivo experiments on 4–6-week-old female BALB/c mice were conducted under the same ethical approval described previously (Ethical Approval No. 82-2022). The weights of the mice were 29 ± 5 g. Mice were shaved using a cordless shaver, and Veet® hair removal cream was applied to yield smooth, hairless skin. Mice were fed and divided into three groups, with each composed of 5 mice; untreated, glimepiride-loaded polymeric microneedles (GLIM_MN), and glimepiride orally administered (GLIM_oral), which was administered by suspending glimepiride nanocrystals with a similar dose to GLIM_MN (132 μg) in 1 mL of distilled water. Glimepiride-loaded microneedles were applied to the mice using a thumb press, and fixed to the skin using adhesive tape (Sellotape®) to avoid expulsion. At predefined time points, the lateral tail vein was punctured. The mice blood was then applied on Accu-check strips and inserted in an Accu-check active glucometer to measure the blood glucose concentration (BG), and the reading was recorded. Mice were fed after 5 hours, monitored for glucose for 24 hours, and were euthanized after 48 hours. Analysis of serum insulin was conducted using a Murine insulin ELISA kit (ELK Biotechnology, USA). Briefly, the collected blood samples from the four groups (GLIM_MN, GLIM_oral, untreated, and Blank_MN) were allowed to clot in a serum separator tube for two hours at room temperature, and then centrifuged for 20 minutes at 1000×g. The analysis of the samples was conducted according to the manufacturer's instructions. Analysis of C-reactive protein was conducted using ELISA (ELK biotechnology, USA). Mice groups were structured in a similar manner to the insulin experiment study with the addition of a positive control group, which was treated with 1 mL of 1% w/v carrageenan solution in PBS (pH 7.4). After 8 hours from administration, blood samples were collected from the groups and processed similarly to the serum insulin study before quantification with the Murine CRP ELISA kit (ELK biotechnology, USA), according to the manufacturer's instructions. Mice were monitored for their survival for 48 hours before euthanasia.

2.11. Statistical analysis

Results were presented as the mean ± standard deviation. Samples were tested using a two-tailed Student's *t*-test for comparison between two groups using GraphPad Prism software (ver. 9; GraphPad, Inc., San Diego, CA, USA). Rejection of the null hypothesis was considered when the p-value < 0.05.

## 3. Results and discussions

3.1. Characterization of glimepiride nanocrystals

Two surfactants, PVP and SLS, were employed to help stabilize the size of the nanocrystals. As shown in Fig. 1(a), nanocrystals prepared using SLS exhibited significantly small size at the same concentration as shown by comparing the size of the 0.2% SLS formula with 0.2% PVP. Moreover, the PI for 0.2% PVP was 1, which indicates a broad unsatisfactory particle size distribution. Increasing the PVP concentration in the antisolvent reduced the PI with no significant change in the particle size. Previously, it has been shown that SLS as a stabilizer in the antisolvent resulted in lower particle sizes than PVP or Tween® 80.[27] As expected, glimepiride exhibited a significant reduction (p-value = 0.0002) in particle size after being ground in a mortar
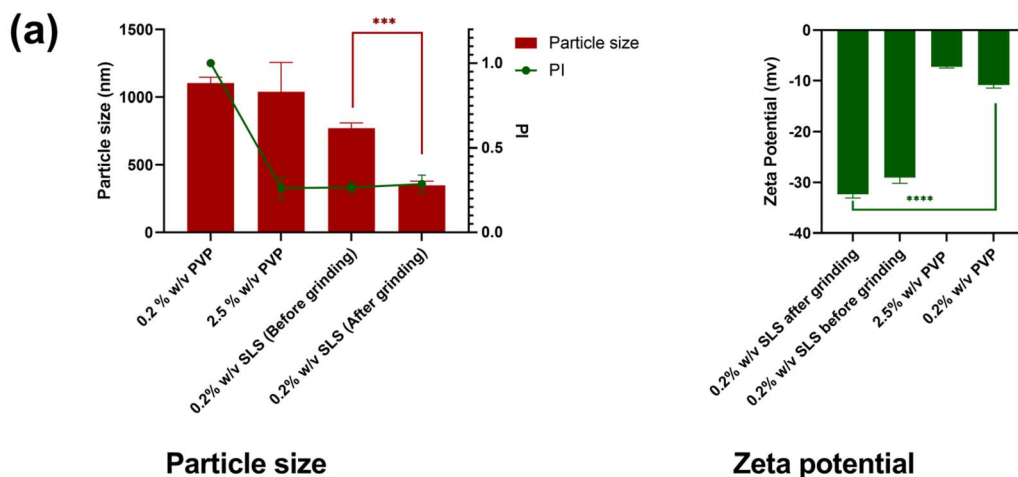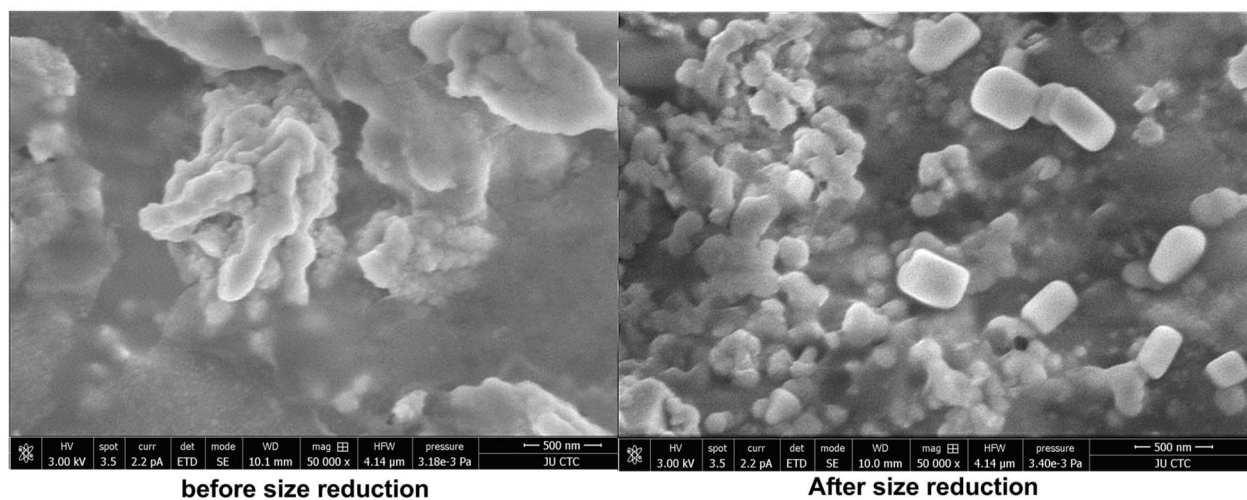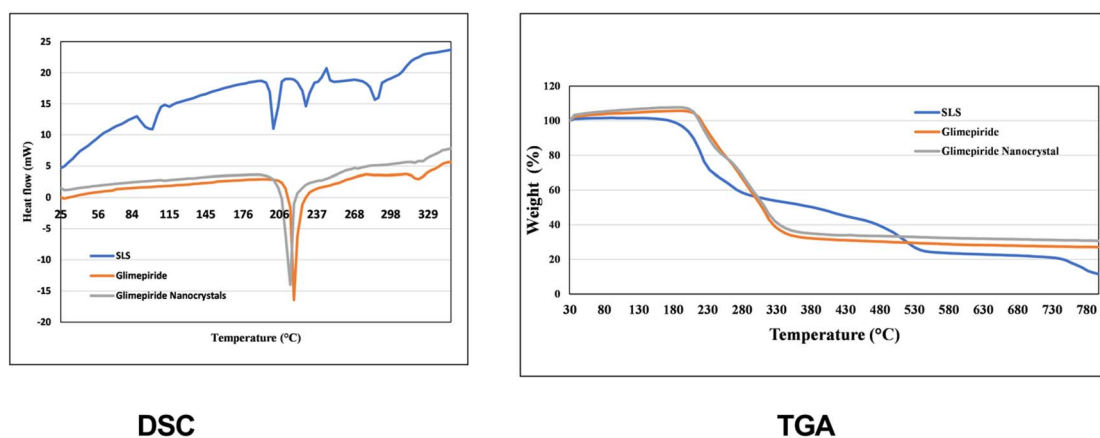
Fig. 1 (a) Particle size and zeta potential for the formulation of 0.2% PVP, 2.5% PVP, and 0.2% SLS as antisolvents before grinding in a mortar and pestle and 0.2% SLS as an antisolvent after grinding in a mortar and pestle, $n = 3$. (b) SEM images of 0.2% SLS before and after grinding. (c) DSC and TGA thermograms for glimepiride powder, ground 0.2% SLS formula, and SLS. ***p-value < 0.001, ****p-value < 0.0001.

and pestle from 772 nm and PI of 0.26 to 348 nm, with no significant change in PI. Therefore, this formula was used for subsequent investigations. These results corroborate a recent study that showed that the size reduction of itraconazole-SLS-hydroxypropyl cellulose with a mortar and pestle for 5 minutes resulted in a significantly lower particle size, with no further improvement at 10 minutes.[28] The size reduction via dry grinding using a mortar and pestle that was employed in our formulation is a versatile, low cost, grinding technique.[29] In contrast, in wet grinding, a levigating agent such as water or other agents is used. Although this technique generates less heat, potential contamination of the particles with the levigating agent is a major problem.[30] As shown in Fig. 1(a), the zeta potential results show a negative zeta potential due to the negatively charged glimepiride.[31] The SEM images for 0.2% SLS before grinding in a mortar and pestle show generally larger particles compared with those after grinding in a mortar and pestle, which corroborate the results obtained from dynamic light scattering (Fig. 1(b)). Many other studies have used a mortar and pestle in the preparation of nanoparticles to achieve the desirable reduced narrow size distribution.[32–34] The differential scanning calorimetry (DSC) thermogram revealed the melting peak at 210 °C for the glimepiride powder (Fig. 1(c)). A similar thermogram appeared for the glimepiride nanocrystal with a melting peak at approximately the same temperature, indicating that the process of formulating the nanocrystals did not change the chemical structure of glimepiride. Similar thermogram behavior with only a single endothermic peak at 210 °C was found in previous studies.[35,36] Thermogravimetric analysis (TGA) revealed a decomposition of glimepiride that started at 226 °C (Fig. 1(c)), similar to a previous study that showed a similar decomposition at that temperature.[37]

3.2. Physical characterization of glimepiride dissolving microneedles

Studying the SEM images of GLIM_MN (size-reduced glimepiride loaded PVA/sucrose) showed an array of pyramidal-shaped microneedles (Fig. 2(a)), and a height of 500 ± 14 μm with sharp tips for GLIM_MN. Moreover, GLIM_MN showed a microneedle base length of 176 ± 4 μm, and a glimepiride entrapment of 132 ± 19 μg per array (Table 1). Such a sharp tip is expected to enhance the smooth penetration capabilities of the microneedle array.[38]

Despite a slight deformation at their tips, the microneedles showed no significant change in their height after application of 32 N for force at 0.5 mm s^{-1} (Fig. 2(b)). The force required for effective human skin penetration is 0.058 N/needles,[39] which is 13.05 N for our microneedle array. Therefore, our formulation can withstand the required insertion force for effective penetration without damage.

3.3. Penetration capabilities of glimepiride-loaded dissolving microneedles

Studying the Parafilm penetration revealed that GLIM_MN was able to fully penetrate the first and second layers of the stacked Parafilm layers (Fig. 3(a) and (b)). Parafilm has been utilized to study the insertion properties of microneedles and their mechanical properties, which resemble human skin and porcine skin.[40] Parafilm is composed of paraffin waxes and polyolefin, and therefore resembles the hydrophobic nature of the stratum corneum.[41] Moreover, the penetration of microneedles through the Parafilm was previously shown to be close in depth to the penetration in neonatal porcine skin.[42] A significant proportion of microneedles were able to penetrate three layers of Parafilm. Each layer is 130 μm thickness; therefore, microneedles penetrated up to a 390 μm depth. In our study, GLIM_MN exhibited full penetration of the array on shaved mice skin (Fig. 3(c)), and the penetration depth was 480 ± 15 μm, as shown by H&E staining (Fig. 3(d)). Moreover, methylene blue microneedles also showed full penetration of the shaved human skin (Fig. 3(e)) and the penetration depth was 276 ± 65 μm, as shown by H&E staining (Fig. 3(f)). Microneedle penetration into human skin is significantly less than the penetration depth of mice skin due to the histological and physiological differences in the skin between mice and human. The human skin stratum corneum thickness is 10 to 20 μm compared to 5 μm for mice.[43] Moreover, the density of hair follicles in mice is higher than human skin, which can serve as natural channels.[44] Collectively, these factors result in a lower penetration depth for microneedles in human skin compared to mice.

3.4. In vitro release and dissolution of glimepiride-loaded dissolving microneedles

The in vitro release of glimepiride from GLIM_MN showed a gradual and complete release by 6 hours (Fig. 4). Studies utilizing Franz cells have demonstrated that DMNs can achieve sustained and gradual drug release when applied to excised mice skin, with release profiles often extending over hours to days depending on the polymers used in the formulations, the inclusion of nanocrystals in the microneedles, and the physicochemical properties of the incorporated drug.[45]

Dissolving microneedles are an innovative drug delivery system designed to painlessly penetrate the skin and rapidly dissolve, releasing therapeutic agents. In studies on rodents, these microneedles have demonstrated quick dissolution upon insertion, efficiently delivering their payload into the skin within minutes.[46] This rapid dissolution enhances drug absorption while minimizing skin irritation, making them a promising alternative to traditional injections. Unlike oral administration, transdermal microneedles bypass the gastrointestinal tract and hepatic first-pass metabolism, potentially reducing variability in drug absorption and enhancing systemic bioavailability of the intact parent drug.[47] Moreover, the minimally invasive nature of microneedles supports improved patient compliance, particularly among populations with swallowing difficulties, or aversion to injections.[48] The GLIM_MNs formulation may also reduce gastrointestinal side effects commonly associated with oral glimepiride, such as nausea or gastric irritation. Additionally, the microneedle platform offers the potential for sustained drug release, providing a steady plasma concentration and minimizing fluctuations that can
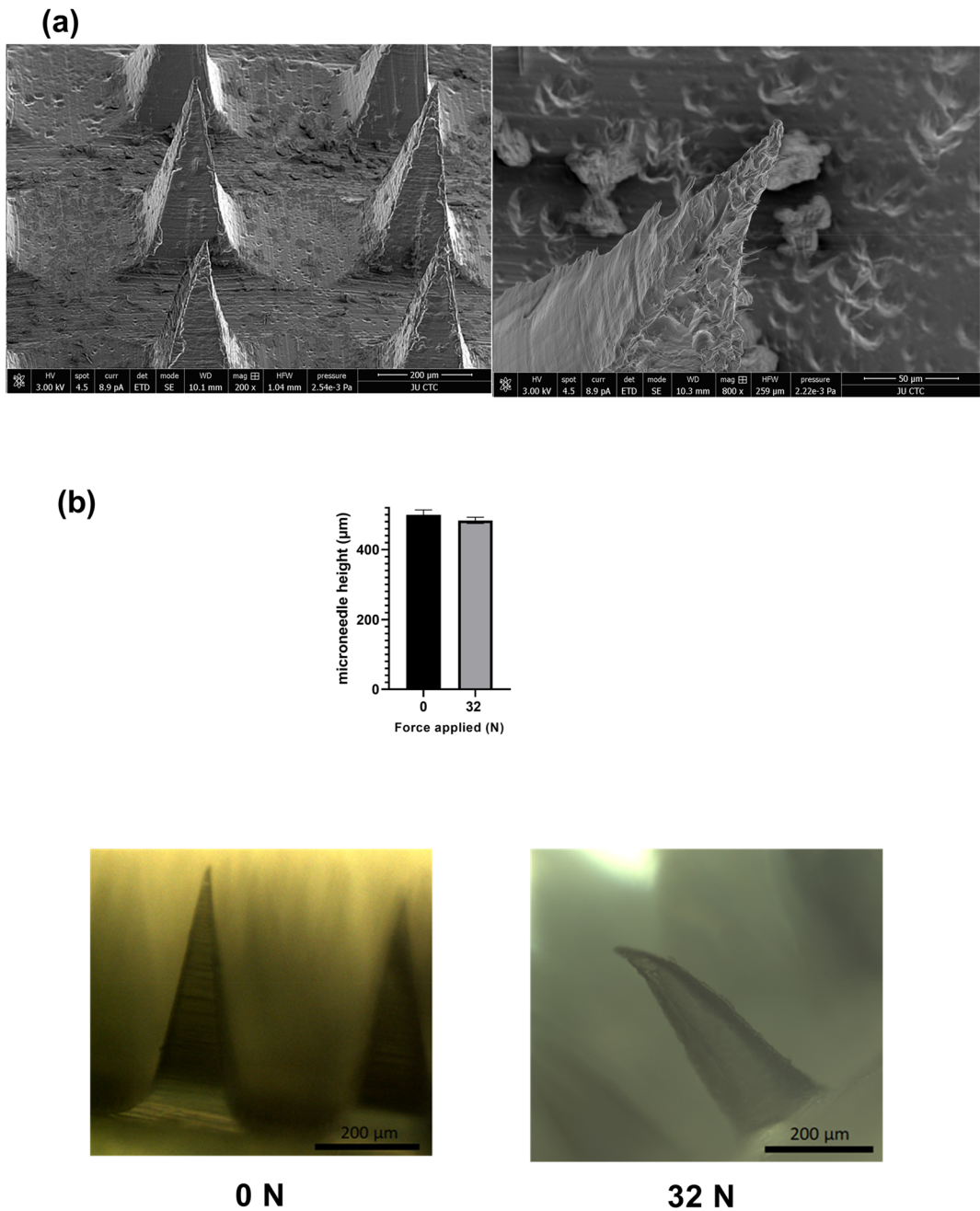
Fig. 2   (a) SEM microscopic images of GLIM_MN, and (b) GLIM_MN height and bright field microscopic images before and after texture analyzer analysis, $n = 3$.

Table 1   Physical characteristics of GLIM_MN: height, base length, glimepiride content, penetration in the excised mice and human skin, $n = 3$

Formula	Microneedles height (µm)	Microneedles height (µm) after texture analyzer	Microneedles base length (µm)	Glimepiride content per array (µg per array)	Excised mice skin penetration depth (µm)	Excised human skin penetration depth (µm)
GLIM_MN	500 ± 14	484 ± 9	176 ± 4	132 ± 19	480 ± 15	276 ± 65

lead to hypoglycemic episodes.[49] These advantages position the microneedle system as a promising alternative for long-term diabetes management, particularly in patient-centric and home-based care settings. In our study, the heights of GLIM_MN gradually decreased in length when incubated in excised mice skin and required 20 minutes to fully dissolve
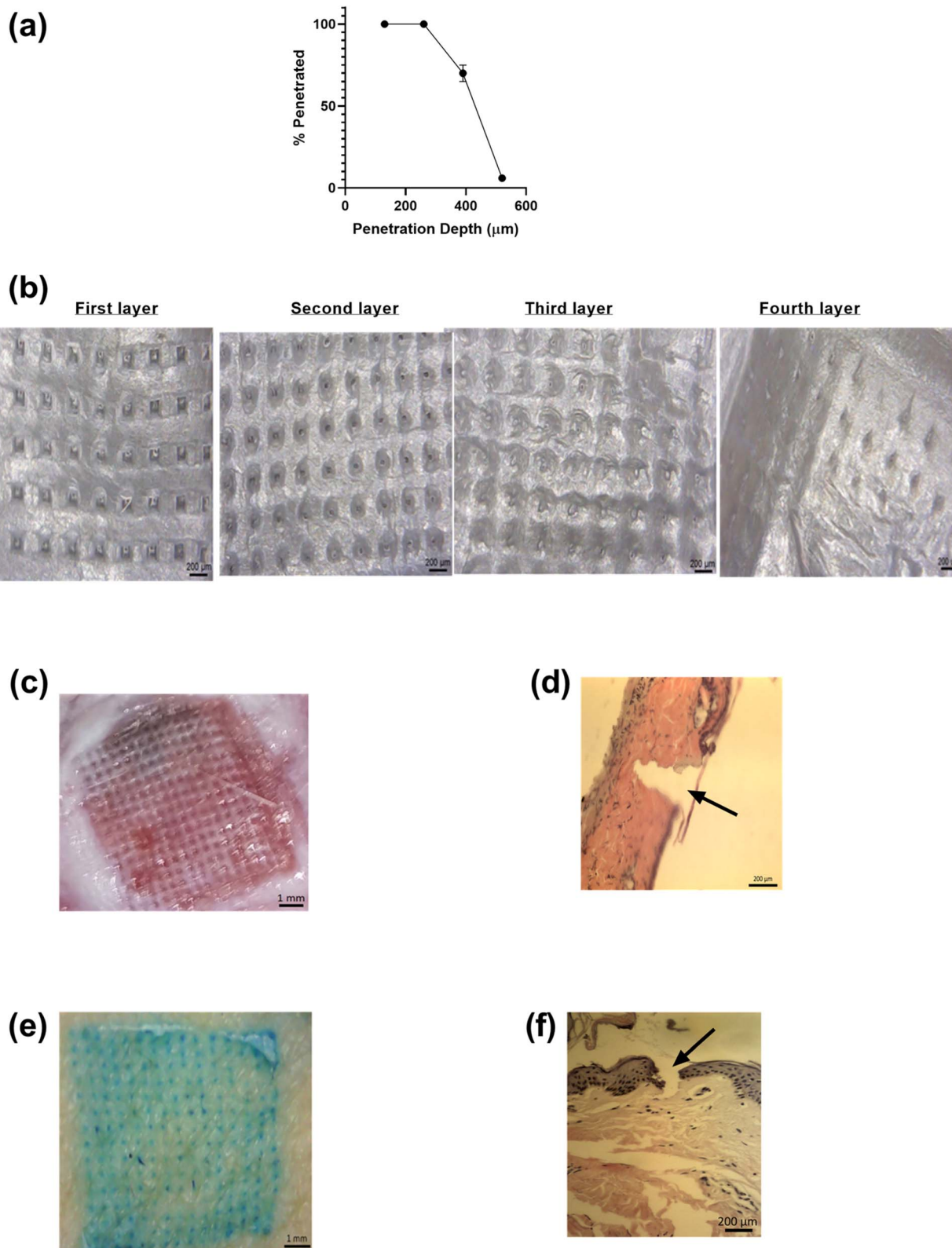
Fig. 3 Penetration of GLIM_MN. (a) Parafilm penetrated vs. penetration depth. (b) Digital light microscopic images of the first through fourth layers of Parafilm. (c) Digital light microscopy image of the excised murine BALB/c skin. (d) Penetration depth of GLIM_MN in the excised mice skin using fluorescence microscopy (bright field). (e) Digital light microscopy image of the excised human skin. (f) Penetration depth of GLIM_MN in the excised human skin using fluorescence microscopy (bright field), $n = 3$.
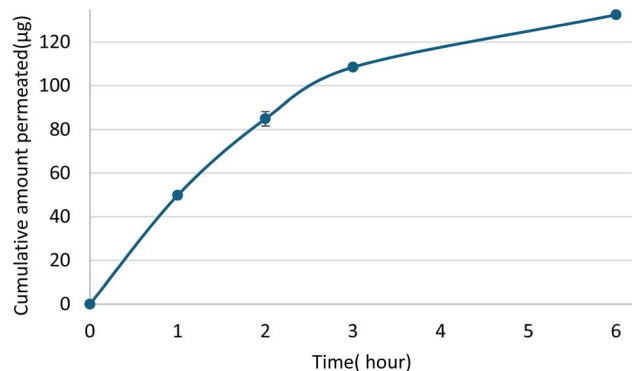
Fig. 4 *In vitro* release of glimepiride from GLIM_MN through full thickness murine skin, $n = 4$.

(Fig. 5(a) and (b)). Dissolving microneedles are based on the dissolution of the polymer in the skin to release the encapsulated drug.[50] Previous studies have shown that PVA-based microneedles can dissolve in excised skin in 60 min or less.[51,52] A previous study of polyvinylpyrrolidone and hyaluronic acid incorporating propranolol had shown a comparable dissolution time of 20 min.[53]

Incorporating glimepiride as nanocrystals within microneedles offers several advantages over its bulk form, particularly in terms of solubility, stability, and release kinetics. Nanocrystals significantly enhance the apparent solubility of the drug and dissolution rate due to their increased surface area, which is especially beneficial for poorly water-soluble drugs like glimepiride.[54,55] Unlike amorphous forms, nanocrystals also offer improved physical and chemical stability, minimizing the risk of recrystallization and degradation during storage or after

administration.[56] Moreover, nanocrystalline formulations can enable more controlled and sustained drug release, which is desirable for achieving prolonged therapeutic levels through the transdermal route.[57] These characteristics collectively justify the use of nanocrystals over bulk glimepiride in the microneedle platform, aiming to improve both bioavailability and patient compliance.

3.5. Antidiabetic activity of glimepiride-loaded PVA/sucrose microneedles

In our study, both GLIM_MN and GLIM_oral showed significantly less blood glucose levels compared to the untreated group (p-value < 0.0001), with a maximum blood glucose lowering effect after 5 hours from administration (Fig. 6(a)). This confirms that intact glimepiride passed from the epidermis to the dermis, where blood capillaries can transport the drug for systemic effect. Both GLIM_oral and GLIM_MN treated groups showed an increase in the serum insulin level at 5 hours (Fig. 6(b)). The blood glucose levels for the GLIM_oral treated group were less than those of the GLIM_MN treated group within the first two hours post-administration (p-value = 0.0005). The higher hypoglycemic effect for GLIM_oral at early time points is due to glimepiride being subjected to oxidative biotransformation primarily *via* the CYP2C9 enzyme, which is abundant in the gastrointestinal tract and liver, resulting in the formation of its active metabolite (M1).[58] This pre-systemic metabolism can contribute to a more rapid pharmacodynamic response after oral dosing. In contrast, the transdermal microneedle route bypasses the gastrointestinal tract and first-pass metabolism, requiring the parent drug to reach systemic circulation before undergoing hepatic metabolism.[59] This delay in biotransformation may plausibly account for the relatively

(a)

(b)

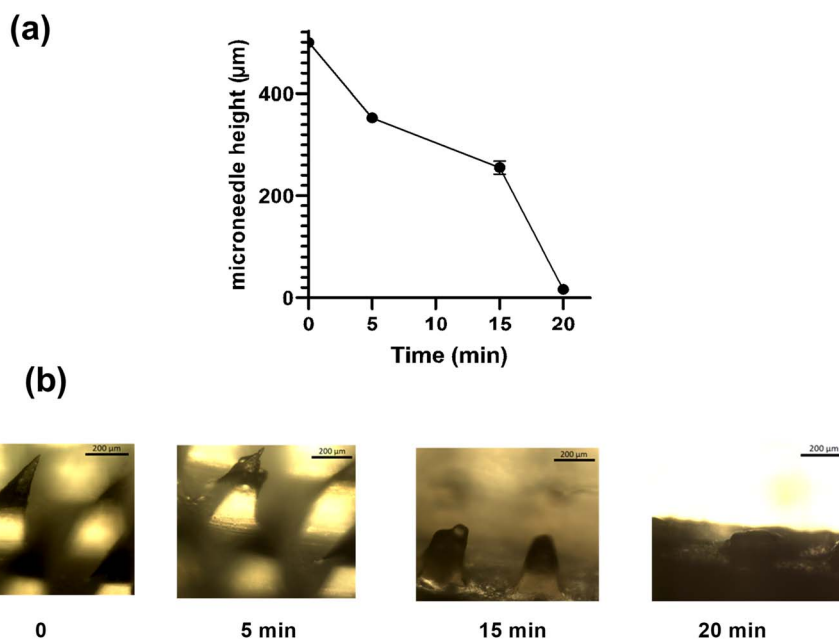

| 0 | 5 min | 15 min | 20 min |

Fig. 5 (a) The microneedles' height *vs.* time after application on the excised mice skin. (b) Bright field images of microneedles at different time points after application on the excised mice skin, $n = 3$.
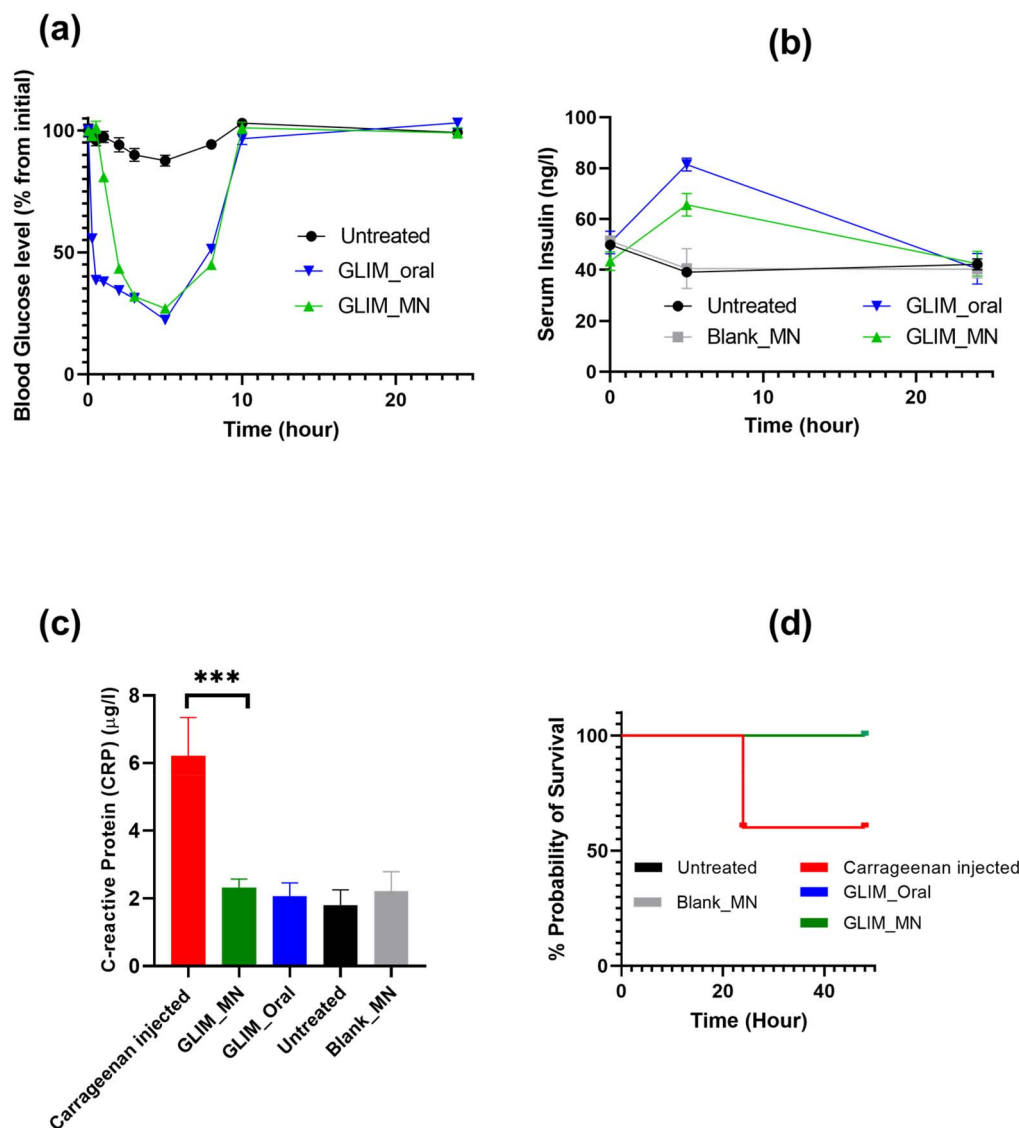
Fig. 6 (a) Blood glucose serum level (% from initial) for GLIM_MN treated, GLIM_oral treated, and untreated BALB/c mice. (b) Serum insulin level for GLIM_MN treated, GLIM_oral treated, Blank_MN treated, and untreated BALB/c mice. (c) Serum C-reactive protein for carrageenan treated, GLIM_MN treated, GLIM_oral treated, Blank_MN treated, and untreated BALB/c mice. (d) The probability of survival for carrageenan treated, GLIM_MN treated, GLIM_oral treated, Blank_MN treated, and untreated BALB/c mice, $n = 5$.

slower onset observed with microneedle delivery, despite the typically rapid absorption profile associated with the transdermal route. Therefore, the delayed effect may be more closely related to differences in metabolic activation rather than solely to absorption kinetics, which was substantiated by the higher insulin levels for GLIM_oral compared to GLIM_MN at 5 hours.

Glimepiride has a T_{max} of 2-3 hours following a single oral dose in humans.[60] Moreover, in a previous study, the maximal insulin and glucose-lowering activity for oral glimepiride was achieved after 2–3 hours, following oral glimepiride dose in type 2 diabetic patients.[61] In our study on BALB/c mice, the maximum glucose-lowering occurred at 5 hours. This is probably due to the higher metabolic rates of mice and differences in enzymatic activity of mice compared to humans.[62] These species-specific metabolic pathways can alter the rate at which

a drug is processed and eliminated, influencing its pharmacokinetic profile, including T_{max}. Moreover, the administration of glimepiride without food for the first 5 hours may explain the continued decline in blood glucose levels during this period.

C-reactive protein (CRP) is a key inflammation biomarker, produced by the liver in response to cytokines like IL-6 and TNF-α.[63] Its rapid elevation makes it useful for assessing inflammatory responses to microneedles (MNs), which penetrate the skin for drug delivery with minimal pain, although their potential to cause inflammation must be evaluated despite the aim to reduce tissue damage.[47,64] Monitoring CRP post-application helps determine whether different MN types trigger excessive immune responses. Our study showed no significant difference between the GLIM_MN treated group and the untreated group, Blank_MN, or GLIM_oral groups

(Fig. 6(c)). The only group that exhibited a significant increase in the C-reactive protein was the carrageenan-treated group. In the carrageenan-treated group, two of the five mice died presumably because of inflammation, and the rest of the mice survived the entire course of study (Fig. 6(d)). Carrageenan has been used to induce inflammation in mice and can elevate the serum C-reactive protein levels.[65] Therefore, our results demonstrate that our microneedle formulation promotes minimal tissue damage and no proinflammatory response. Previously, it has been shown that dissolving microneedles using biocompatible polymers, including polyvinyl pyrrolidone, maintains skin integrity and does not trigger inflammation.[66]

The maximum daily dose of glimepiride is 8 mg per day, and the effective concentration is 0.5–8 mg per day.[58] Such a potent dose is advantageous, as high doses may limit the usefulness for dissolving microneedle drug delivery since they can entrap only small doses due to their diminutive structure.[16] Moreover, glimepiride is a second-generation sulfonylurea that is more potent and has fewer side effects than first-generation sulfonylurea.[67] Therefore, incorporating glimepiride into dissolving microneedles has great potential in reducing blood glucose levels in type 2 diabetes mellitus.

Previously, glimepiride was incorporated in a nanoemulgel formulation to enhance its transdermal permeation since it has low skin permeation.[68] Other transdermal formulations of glimepiride complexes have also shown improved transdermal delivery as an alternative to oral delivery.[69,70] These studies aimed at modifying the formulation, allowing for efficient transdermal delivery. Therefore, it was postulated that actively puncturing and penetrating the stratum corneum, the main skin barrier, can improve the antidiabetic effect of glimepiride.

Regulatory authorities such as the U.S. FDA are increasingly expected to require sterility for polymeric microneedle patches, especially when used for the transdermal delivery of systemic therapeutics, vaccines, or biologics, due to the potential risk of skin infections and microbial contamination.[71,72] This requirement introduces manufacturing and distribution challenges, including the need for aseptic processing or terminal sterilization methods such as gamma irradiation treatment that do not compromise the microneedle's mechanical or chemical integrity.[73] Ensuring storage stability is also critical, particularly in maintaining the performance of PVA or other polymeric platforms used in microneedle formulations under various environmental conditions, which may require desiccants or cold-chain storage depending on the formulation.[74,75] Studies have shown that microneedle patches can reliably penetrate the stratum corneum (outer skin layer) with forces as low as 5–10 N, meaning that a normal thumb press is sufficient for effective application in many cases.[76,77] This is evident as our microneedle formulation fully penetrated the Parafilm, mice skin, and human skin. For reproducible insertion, self-administration by patients or caregivers raises concerns about consistent skin penetration and dose delivery. However, if applied by thumb press, users may utilize feedback mechanisms such as color changes, which are being explored to confirm proper use.[78] In our study, color change was used in methylene blue-loaded microneedles to confirm efficient

delivery to excised human skin. Dissolving microneedles, depending on their design and material, generally dissolve and release their payload within minutes to days, and can be used for immediate or sustained transdermal delivery.[16] Disposal is another important consideration, especially in resource-poor settings, where the lack of sharps containers or proper waste management systems could lead to environmental contamination or safety risks. To address this, biodegradable or dissolving microneedles that leave no sharp waste are increasingly favored for safe, low-resource deployment.[79]

4. Conclusion

In this work, we successfully developed a robust formulation of glimepiride nanocrystals into PVA/sucrose-based dissolving microneedles. The dose of glimepiride incorporated into the microneedles was adequate to lower blood glucose levels and increase serum insulin levels in mice. Moreover, our microneedle formulation punctured and penetrated human skin and penetrated mice skin without triggering inflammation. Microneedles offer a promising alternative for delivering drugs with poor skin permeability, such as glimepiride, by enabling systemic absorption, reducing blood glucose levels, boosting insulin production, and avoiding inflammation. This minimally invasive method addresses the key challenges of oral antidiabetic delivery and provides additional benefits, including better patient adherence (especially for patients with dysphagia), avoidance of gastrointestinal side effects, and the possibility of sustained drug release.

Author contributions

Conceptualization, S. A. and A. A.; methodology S. A., W. A., A. A., H. A., and O. A.; software, S. A. and A. A; validation, W. A., S. A., and A. A.; formal analysis, S. A., A. A., W. A., and Y. A.; investigation, S. A.; resources, W. A., S. A., S. J., R. B., H. A., and O. A.; data curation, S. A., W. A., and A. A.; writing – original draft preparation, S. A. and A. A., W. A., and Y. A.; writing – review and editing, S. A., W. A., and A. A.; visualization, S. A.; supervision, S. A. and W. A.; project administration, S. A.; funding acquisition, S. A. All the authors have read and agreed to the published version of the manuscript.

Conflicts of interest

The authors declare no conflict of interest.

Acknowledgements

References

1 I. D. Federation, *IDF Diabetes Atlas* 10th edn, 2021.
2 Y. Zheng, S. H. Ley and F. B. Hu, *Nat. Rev. Endocrinol.*, 2018, **14**, 88–98.

3   Z. H. Israili, *Am. J. Ther.*, 2011, **18**, 117–152.

4   D. K. Song and F. M. Ashcroft, *Br. J. Pharmacol.*, 2001, **133**, 193–199.

5   A. L. McCall, *Expert Opin. Pharmacother.*, 2001, **2**, 699–713.

6   V. J. Briscoe, M. L. Griffith and S. N. Davis, *Expert Opin. Drug Metab. Toxicol.*, 2010, **6**, 225–235.

7   A. Basit, M. Riaz and A. Fawwad, *Vasc. Health Risk Manage.*, 2012, **8**, 463–472.

8   F. Becić, E. Kapić and E. Becić, *Med. Arh.*, 2003, **57**, 125–127.

9   A. Ahad, A. A. Al-Saleh, N. Akhtar, A. M. Al-Mohizea and F. I. Al-Jenoobi, *Drug Discovery Today*, 2015, **20**, 1217–1227.

10 L. C. Ng and M. Gupta, *Asian J. Pharm. Sci.*, 2020, **15**, 13–25.

11 P. Khanna, J. A. Strom, J. I. Malone and S. Bhansali, 2008, **2**, 1122–1129.

12 J. Yu, Y. Zhang, Y. Ye, R. DiSanto, W. Sun, D. Ranson, F. S. Ligler, J. B. Buse and Z. Gu, *Proc. Natl. Acad. Sci. U. S. A.*, 2015, **112**, 8260–8265.

13 B. A. Jana and A. D. Wadhwani, *Indian J. Pharmacol.*, 2019, **51**, 4–10.

14 X. Jin, D. D. Zhu, B. Z. Chen, M. Ashfaq and X. D. Guo, *Adv. Drug Delivery Rev.*, 2018, **127**, 119–137.

15 T. Liu, G. Jiang, G. Song, Y. Sun, X. Zhang and Z. Zeng, *J. Pharm. Sci.*, 2021, **110**, 3004–3010.

16 J. W. Lee, J. H. Park and M. R. Prausnitz, *Biomaterials*, 2008, **29**, 2113–2124.

17 E. Proksch, J. M. Brandner and J.-M. Jensen, *Exp. Dermatol.*, 2008, **17**, 1063–1072.

18 K. Ita, *Biomed. Pharmacother.*, 2017, **93**, 1116–1127.

19 Z. Sartawi, C. Blackshields and W. Faisal, *J. Controlled Release*, 2022, **348**, 186–205.

20 A. Akram, A. Kiran and S. Naeem, *J. Contemp. Pharm.*, 2019, **3**, 1–6.

21 B. Lorenzati, C. Zucco, S. Miglietta, F. Lamberti and G. Bruno, *Pharmaceuticals*, 2010, **3**, 3005–3020.

22 F. Moawad, R. Pouliot and D. Brambilla, *J. Controlled Release*, 2025, **383**, 113794.

23 A. Reinke, E. J. Whiteside, L. Windus, D. Desai, E. Stehr and Z. Faraji Rad, *Biomed. Eng. Adv.*, 2024, **8**, 100127.

24 S. Duarah, M. Sharma and J. Wen, *Eur. J. Pharm. Biopharm.*, 2019, **136**, 48–69.

25 A. B. Mohd, K. Sanka, R. Gullapelly, P. V. Diwan and N. Shastri, *J. Anal. Sci. Technol.*, 2014, **5**, 27.

26 R. S. H. Mansour, Hamdan II, M. S. H. Salem, E. A. Khalil and A. A. Sallam, *PLoS One*, 2021, **16**, e0247879.

27 S. Abdelghany, I. A. Tekko, L. Vora, E. Larrañeta, A. D. Permana and R. F. Donnelly, *Pharmaceutics*, 2019, **11**, 308.

28 A. Coelho, L. Schenck, G. Guner, A. Punia and E. Bilgili, *Powders*, 2022, **1**, 88–110.

29 M. Y. Thong, Y. J. Manrique and K. J. Steadman, *PLoS One*, 2018, **13**, e0193683.

30 S. C. Chelgani, M. Parian, P. S. Parapari, Y. Ghorbani and J. Rosenkranz, *J. Mater. Res. Technol.*, 2019, **8**, 5004–5011.

31 A. Pal, S. Roy, A. Kumar, S. Mahmood, N. Khodapanah, S. Thomas, C. Agatemor and K. Ghosal, *ACS Omega*, 2020, **5**, 19968–19977.

32 F. Rashidashmagh, Y. Doekhi-Bennani, M. Tizghadam-Ghazani, J. P. van der Hoek, A. Mashayekh-Salehi, B. S. G. J. Heijman and K. Yaghmaeian, *J. Hazard. Mater.*, 2021, **404**, 124154.

33 K. P. Reddy, R. S. Meerakrishna, P. Shanmugam, B. Satpati and A. Murugadoss, *New J. Chem.*, 2021, **45**, 438–446.

34 A. Murugadoss, N. Kai and H. Sakurai, *Nanoscale*, 2012, **4**(4), 1280–1282.

35 M. Nagpal, R. Rajera, K. Nagpal, P. Rakha, S. Singh and D. Mishra, *Int. J. Pharm. Invest.*, 2012, **2**, 42–47.

36 A. Mehta, S. Vasanti, R. Tyagi and A. Shukla, *Curr. Trends Biotechnol. Pharm.*, 2009, **3**, 76–84.

37 N. S. Riyaz and I. Badran, *J. Therm. Anal. Calorim.*, 2022, **147**, 10755–10765.

38 A. M. Römgens, D. L. Bader, J. A. Bouwstra, F. P. T. Baaijens and C. W. J. Oomens, *J. Mech. Behav. Biomed. Mater.*, 2014, **40**, 397–405.

39 J. D. Kim, M. Kim, H. Yang, K. Lee and H. Jung, *J. Controlled Release*, 2013, **170**, 430–436.

40 J. Ziesmer, P. Tajpara, N. J. Hempel, M. Ehrström, K. Melican, L. Eidsmo and G. A. Sotiriou, *Adv. Mater. Technol.*, 2021, **6**, 2001307.

41 J. Wang, R. Chen, M. Ma and L. Li, *Anal. Chem.*, 2008, **80**, 491–500.

42 E. Larrañeta, J. Moore, E. M. Vicente-Pérez, P. González-Vázquez, R. Lutton, A. D. Woolfson and R. F. Donnelly, *Int. J. Pharm.*, 2014, **472**, 65–73.

43 J. C. J. Wei, G. A. Edwards, D. J. Martin, H. Huang, M. L. Crichton and M. A. F. Kendall, *Sci. Rep.*, 2017, **7**, 15885.

44 G. Salgado, Y. Z. Ng, L. F. Koh, C. S. M. Goh and J. E. Common, *Differentiation*, 2017, **98**, 14–24.

45 T. Bauleth-Ramos, N. El-Sayed, F. Fontana, M. Lobita, M.-A. Shahbazi and H. A. Santos, *Mater. Today*, 2023, **63**, 239–287.

46 M.-H. Ling and M.-C. Chen, *Acta Biomater.*, 2013, **9**, 8952–8961.

47 M. R. Prausnitz and R. Langer, *Nat. Biotechnol.*, 2008, **26**, 1261–1268.

48 F. K. Aldawood, A. Andar and S. Desai, *Polymers*, 2021, **13**, 2815.

49 E. McAlister, M. Kirkby, J. Domínguez-Robles, A. J. Paredes, Q. K. Anjani, K. Moffatt, L. K. Vora, A. R. J. Hutton, P. E. McKenna, E. Larrañeta and R. F. Donnelly, *Adv. Drug Delivery Rev.*, 2021, **175**, 113825.

50 Y. C. Kim, J. H. Park and M. R. Prausnitz, *Adv. Drug Delivery Rev.*, 2012, **64**, 1547–1568.

51 S. Abdelghany, I. A. Tekko, L. Vora, E. Larrañeta, A. D. Permana and R. F. Donnelly, *Pharmaceutics*, 2019, **11**, 308.

52 S. Abdelghany, W. Alshaer, Y. Al Thaher, M. Al Fawares, A. G. Al-Bakri, S. Zuriekat and R. S. Mansour, *Beilstein J. Nanotechnol.*, 2022, **13**, 517–527.

53 J. He, Z. Zhang, X. Zheng, L. Li, J. Qi, W. Wu and Y. Lu, *Pharmaceutics*, 2021, **13**, 579.

54 V. B. Patravale, A. A. Date and R. M. Kulkarni, *J. Pharm. Pharmacol.*, 2004, **56**, 827–840.

55 R. H. Müller, S. Gohla and C. M. Keck, *Eur. J. Pharm. Biopharm.*, 2011, **78**, 1–9.

56 R. Shegokar and R. H. Müller, *Int. J. Pharm.*, 2010, **399**, 129–139.

57 C. M. Keck and R. H. Müller, *Eur. J. Pharm. Biopharm.*, 2006, **62**, 3–16.

58 H. D. Langtry and J. A. Balfour, *Drugs*, 1998, **55**, 563–584.

59 V. Phatale, K. K. Vaiphei, S. Jha, D. Patil, M. Agrawal and A. Alexander, *J. Controlled Release*, 2022, **351**, 361–380.

60 G. Müller, D. Hartz, J. Pünter, R. Okonomopulos and W. Kramer, *Biochim. Biophys. Acta*, 1994, **1191**, 267–277.

61 R. B. Goldberg, S. M. Holvey and J. Schneider, *Diabetes Care*, 1996, **19**, 849–856.

62 A. K. MacLeod, K. S. Coquelin, L. Huertas, F. R. C. Simeons, J. Riley, P. Casado, L. Guijarro, R. Casanueva, L. Frame, E. G. Pinto, L. Ferguson, C. Duncan, N. Mutter, Y. Shishikura, C. J. Henderson, D. Cebrian, C. R. Wolf and K. D. Read, *Proc. Natl. Acad. Sci. U. S. A.*, 2024, **121**, e2315069121.

63 M. B. Pepys and G. M. Hirschfield, *J. Clin. Invest.*, 2003, **111**, 1805–1812.

64 S. Black, I. Kushner and D. Samols, *J. Biol. Chem.*, 2004, **279**, 48487–48490.

65 E. Vazquez, M. Navarro, Y. Salazar, G. Crespo, G. Bruges, C. Osorio, V. Tortorici, H. Vanegas and M. López, *Inflammation Res.*, 2015, **64**, 333–342.

66 E. M. Vicente-Perez, E. Larrañeta, M. T. C. McCrudden, A. Kissenpfennig, S. Hegarty, H. O. McCarthy and R. F. Donnelly, *Eur. J. Pharm. Biopharm.*, 2017, **117**, 400–407.

67 I. Sahin, O. Bakiner, T. Demir, R. Sari and A. Aysegul, *Diabetes Ther.*, 2024, **15**, 1687–1716.

68 F. A. Razzaq, M. Asif, S. Asghar, M. Iqbal, I. U. Khan, S.-u.-D. Khan, M. Irfan, H. K. Syed, A. A. Khames, H. Mahmood, A. Y. Ibrahim and A. M. El Sisi, *Cells*, 2021, **10**, 2404.

69 H. Li, J. Wang, Q. Xu, S. Tian and W. Yang, *Drug Dev. Ind. Pharm.*, 2022, **48**, 397–405.

70 H. O. Ammar, H. A. Salama, S. A. El-Nahhas and H. Elmotasem, *Curr. Drug Delivery*, 2008, **5**, 290–298.

71 K. Ita, *Pharmaceutics*, 2015, **7**, 90–105.

72 H. X. Nguyen, *Medicines*, 2025, **12**, 4.

73 M. T. McCrudden, A. Z. Alkilani, A. J. Courtenay, C. M. McCrudden, B. McCloskey, C. Walker, N. Alshraiedeh, R. E. Lutton, B. F. Gilmore, A. D. Woolfson and R. F. Donnelly, *Drug Delivery Transl. Res.*, 2015, **5**, 3–14.

74 M. J. Mistilis, J. C. Joyce, E. S. Esser, I. Skountzou, R. W. Compans, A. S. Bommarius and M. R. Prausnitz, *Drug Delivery Transl. Res.*, 2017, **7**, 195–205.

75 Q. L. Wang, J. W. Ren, B. Z. Chen, X. Jin, C. Y. Zhang and X. D. Guo, *J. Ind. Eng. Chem.*, 2018, **59**, 251–258.

76 E. Larrañeta, R. E. M. Lutton, A. D. Woolfson and R. F. Donnelly, *Mater. Sci. Eng., R*, 2016, **104**, 1–32.

77 E. Larrañeta, J. Moore, E. M. Vicente-Pérez, P. González-Vázquez, R. Lutton, A. D. Woolfson and R. F. Donnelly, *Int. J. Pharm.*, 2014, **472**, 65–73.

78 H. Li, Q. K. Anjani, A. R. J. Hutton, J. L. Paris, N. Moreno-Castellanos, A. Himawan, E. Larrañeta and R. F. Donnelly, *Adv. Healthcare Mater.*, 2024, **13**, 2304082.

79 R. F. Donnelly, M. J. Garland, D. I. J. Morrow, K. Migalska, T. R. R. Singh, R. Majithiya and A. D. Woolfson, *J. Controlled Release*, 2010, **147**, 333–341.